NANO LETTERS

2006
Vol. 6, No. 12
2929−2934

Single p-Type/Intrinsic/n-Type Silicon Nanowires as Nanoscale Avalanche Photodetectors

Chen Yang,[†,§] Carl J. Barrelet,[†,§] Federico Capasso,[‡] and Charles M. Lieber*[,†,‡]

Department of Chemistry and Chemical Biology, Harvard University, Cambridge, Massachusetts 02138, and Division of Engineering and Applied Science, Harvard University, Cambridge, Massachusetts 02138

Received October 2, 2006; Revised Manuscript Received October 19, 2006

ABSTRACT

We report the controlled synthesis of axial modulation-doped p-type/intrinsic/n-type (p-i-n) silicon nanowires with uniform diameters and single-crystal structures. The p-i-n nanowires were grown in three sequential steps: in the presence of diborane for the p-type region, in the absence of chemical dopant sources for the middle segment, and in the presence of phosphine for the n-type region. The p-i-n nanowires were structurally characterized by transmission electron microscopy, and the spatially resolved electrical properties of individual nanowires were determined by electrostatic force and scanning gate microscopies. Temperature-dependent current–voltage measurements recorded from individual p-i-n devices show an increase in the breakdown voltage with temperature, characteristic of band-to-band impact ionization, or avalanche breakdown. Spatially resolved photocurrent measurements show that the largest photocurrent is generated at the intrinsic region located between the electrode contacts, with multiplication factors in excess of ca. 30, and demonstrate that single p-i-n nanowires function as avalanche photodiodes. Electron- and hole-initiated avalanche gain measurements performed by localized photoexcitation of the p-type and n-type regions yield multiplication factors of ca. 100 and 20, respectively. These results demonstrate the significant potential of single p-i-n nanowires as nanoscale avalanche photodetectors and open possible opportunities for studying impact ionization of electrons and holes within quasi-one-dimensional semiconductor systems.

Semiconductor nanowires are emerging as powerful building blocks for the integration of nanophotonic devices on a chip.[1] For example, nanowire-based light-emitting diodes,[2,3] lasers,[4−6] active waveguides,[7] electro-optical modulators,[7a,8] and photodetectors[9,10] have been demonstrated, and more recently, hybrid nanowire−photonic crystal and nanowire−microresonator structures have been reported.[11] The development of high-sensitivity nanoscale photodectors is especially important for the realization of integrated nanophotonic systems, and they could open opportunities in a number of other areas, including optical biosensor systems,[12,13] optofluidic systems, and optical interconnects.[14] To this end we recently reported nanoscale avalanche photodiodes (APDs) consisting of crossed Si−CdS nanowire p-n diodes heterojunctions.[10] APDs are an especially attractive device structure for nanoscale photodetectors because they can enable large photocurrent gain and sensitivity down to the single photon level,[15,16] capabilities that are essential in nanoscale detectors due to their intrinsic small photon collection area.

Complementary doping within a single nanowire versus assembly of two distinctly doped nanowires[10] represents an alternative strategy for preparing nanoscale photodiodes and, moreover, might lead to better defined junctions. Indeed, complementary doping is used extensively to make planar p-type/intrinsic/n-type (p-i-n) structures used in APDs,[15] although to date there have been no reported studies of p-i-n structures in nanowires. Here, we describe the first controlled synthesis and properties of axial modulation-doped p-i-n nanowires. We demonstrate that APDs based on single p-i-n silicon nanowires (SiNWs) can have large photomultiplication and subwavelength spatial resolution for detection. Moreover, we use these devices to characterize the multiplication factors for impact ionization of electrons and holes in p-i-n SiNWs, which suggest that p-i-n nanowire structures will be interesting systems for studying the physics of carrier transport in low-dimensional structures at high electrical fields.

The p-i-n SiNWs were synthesized by the nanocluster-catalyzed chemical vapor deposition approach described previously.[1,17−20] In brief, 20 nm Au nanoclusters were used as catalysts to sequentially grow p-type, undoped, and n-type regions, with silane as the precursor for silicon,

* Corresponding author. E-mail: cml@cmliris.harvard.edu.
† Department of Chemistry and Chemical Biology.
‡ Division of Engineering and Applied Science.
§ These authors contributed equally to this work.

10.1021/nl062314b CCC: $33.50
Published on Web 11/16/2006

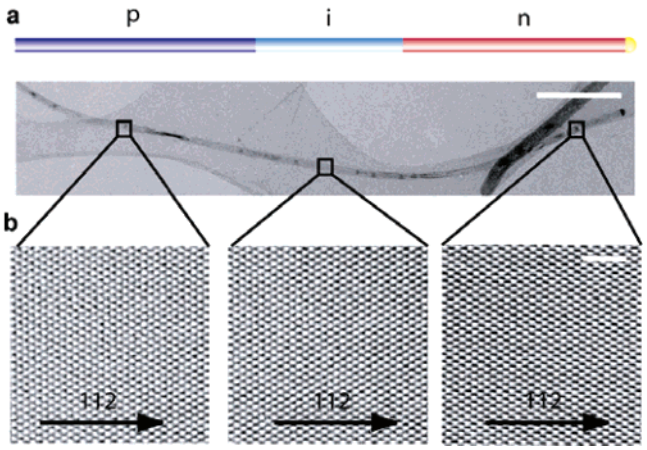

Figure 1. TEM characterization of p-i-n SiNWs. (a) Schematic of a p-i-n NW, where the yellow hemisphere (right end) corresponds to the Au-nanocluster catalyst used in the sequential growth of the p-type (purple), i (pale blue), and n-type (red) regions. Low-resolution TEM image of a representative 20 nm diameter p-i-n SiNW; scale bar is 500 nm. (b) High-resolution TEM images from the p-i-n segments—left, middle, and right, respectively—recorded along the [1,1,−1] zone axis; the images were taken from the central regions indicated by the boxes along the low-resolution SiNW in (a). Scale bar is 2 nm.

diborane for p-type dopants, and phosphine for n-type dopants.[18−20] Synthesis was carried out using a local substrate heater with H_2 as carrier gas to eliminate simultaneous radial growth during axial NW elongation, and on the basis of the growth rates and times, we expect individual p-i-n sections of 2.88−1.08−2.88 μm, respectively.[18] The dopant concentration was varied by controlling the feed-in ratio between silane and phosphine (diborane), and the effective dopant concentrations in the p-type and n-type regions were estimated to be ca. $8 \times 10^{19}/\text{cm}^3$ and ca. $5 \times 10^{19}/\text{cm}^3$, respectively.[19] Synthesis of the undoped region between the p- and n-type regions was achieved by switching off the dopant flow while maintaining axial growth. The effective carrier density of the undoped region, ca. $10^{16}/\text{cm}^3$, is 10^3−10^4 lower than the effective concentration in the p- and n-type regions, and hence we term this section intrinsic. Although the exact dopant number is not known in the SiNWs, it is worth recognizing that a concentration of $10^{16}/\text{cm}^3$ corresponds to only ca. 3 dopants in a 1 μm long 20 nm diameter Si crystal,[19] which is consistent with the assignment of this region as intrinsic.

Low- and high-resolution transmission electron microscopy (TEM) studies of p-i-n SiNWs (e.g., Figure 1) show that NW diameters are very uniform over the lengths of the structures with no observable end-to-end change. These results show that simultaneous radial growth, which would obscure modulation of electronic properties along the nanowire axis,[18] has been effectively eliminated in the growth of the p-i-n SiNWs. The low-resolution TEM and SEM (not shown) data also show that the average p-i-n SiNW length, ca. 6.5 μm, is consistent with the 6.84 μm length expected based on the growth rates/times.[18] In addition, high-resolution TEM images recorded from the p-, i-, and n-regions (Figure 1b) demonstrate that these SiNWs have uniform single-crystalline structures, despite the changes in chemical dopant sources during synthesis, with a ⟨112⟩ lattice direction along the NW axis. The demonstration of single-crystal structures with uniform growth direction is important for studies of APDs, because the multiplication factors may vary for different crystallographic directions.[21,22]

To confirm that SiNWs exhibit expected variations in the electronic properties associated with p-i-n dopant modulation, we used electrostatic force microscopy (EFM) and scanning gate microscopy (SGM).[18,23−25] In these measurements (Figure 2a, top), a conducting tip with applied voltage V_{tip} was scanned at a fixed height over a p-i-n SiNW device with bias V_{sd} applied through contacts to the p- and n-type ends of the NW. We can glean several important points from the resulting data. First, the AFM topography image shows a well-defined single NW device ca. 4.7 μm in length between the contact electrodes. Inclusion of the 1 μm NW lengths under each electrode contact yields a total NW length, ca. 6.7 μm, consistent with the estimated value of 6.8 based on growth. Second, the line-profile of EFM phase-shift signal measured along the p-i-n SiNW axis exhibits a pronounced change only across the middle region of the device and, thus, shows that voltage drop occurs primarily across this ca. 1.0 μm long middle region. Third, the SGM image of the same device further demonstrates a substantial change (decrease) in conductance only in this same 1.0 μm long middle region of the p-i-n SiNW device. The SGM results are consistent with heavily doped end-regions, which do not undergo substantial depletion or accumulation in presence of local tip gate, and a lightly p-type central region, which we refer to as "i" due to the low effective dopant concentration determined from resistivity measurements (see above). Taken together, these results indicate that the i-region of our p-i-n SiNWs has a length of 1.0 ± 0.2 μm, which is consistent with the length estimated from the growth rate and growth time,[18] and that the voltage drops primarily across this region as expected for a well-defined p-i-n structure.

The electrical properties of p-i-n junctions within nanowires were also probed by the current (I) versus bias voltage (V) measurements. Representative data recorded from a p-i-n SiNW device at room temperature (Figure 2c) show current rectification with significant current flowing at a forward bias >1 V. The reverse bias results further show a sharp increase at a much larger voltage, 38 V, that we associate with breakdown voltage (V_{B}). This sharp increase in current at V_{B} is suggestive of an avalanche breakdown mechanism.[15] The corresponding breakdown field, assuming the voltage drop occurs across the i-region is ca. 4×10^5 V/cm. Most of the p-i-n SiNW devices exhibited similar values of V_{B}, indicating good reproducibility in the synthesis of these p-i-n structures. It is also important to note that our devices can sustain high current densities, up to ca. 10^6 A/cm^2, without damage or failure. In addition, we have characterized the temperature of the reverse-bias breakdown behavior (Figure 2d). Significantly, these $I-V$ data show a positive shift in the onset of breakdown with increasing temperature, corresponding to a temperature coefficient of ca. 30 mV/K. A similar positive temperature coefficient was reported recently

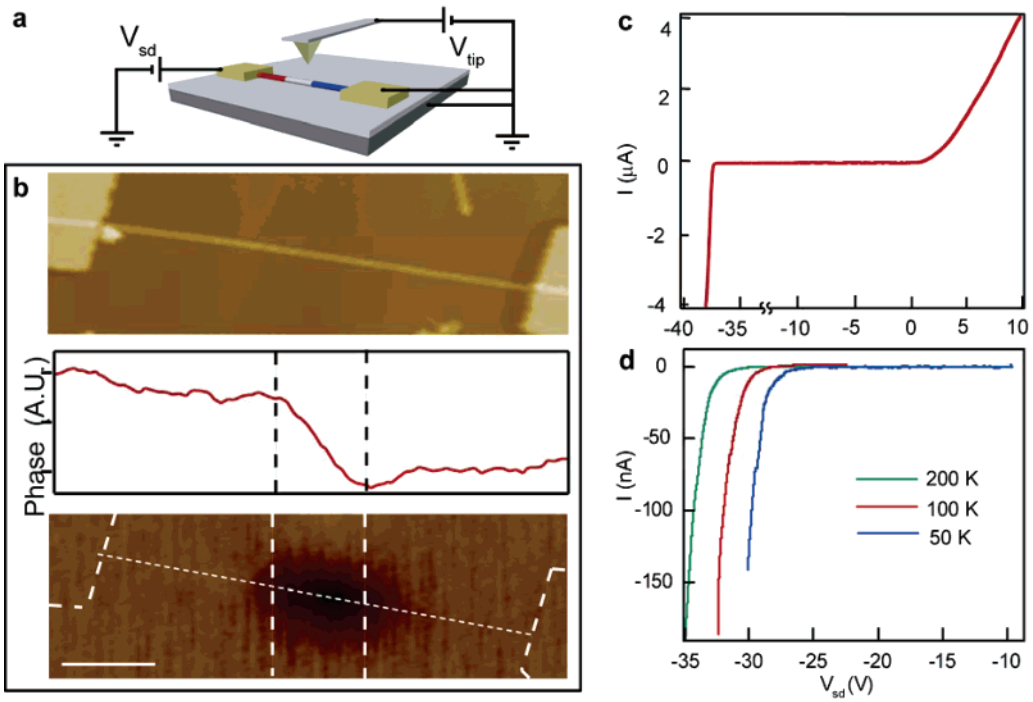

Figure 2. Probe microscopy and transport characteristic of p-i-n SiNW devices. (a) Schematic of the measurement setup. (b) From top to bottom: (i) AFM topograph of the p-i-n SiNW, (ii) plot of EFM phase shift vs position recorded along the nanowire axis, and (iii) SGM image taken on the same device. The dark region corresponds to a decrease in current, white dash lines in the SGM image indicate the p-i-n SiNW between contacts and electrodes. The vertical dash lines mark the intrinsic regions. Scale bar shown in SGM image, 1 μm, is the same for EFM and AFM images. (c) Current vs applied voltage curve for a typical SiNW p-i-n junction at room temperature. (d) Current vs applied reverse voltage data of a p-i-n SiNW recorded at temperature of 200 K (green line), 100 K (red line), and 50 K (blue line).

for p-Si/n-CdS crossed-NW APDs.[10] The measured positive temperature coefficient confirms that the breakdown mechanism is based on band-to-band impact ionization rather than on band-to-band tunneling,[15] that is, avalanche breakdown.

To characterize the optoelectronic properties of the SiNW p-i-n junctions and evaluate their potential as nanoscale APDs, we have combined a scanning optical microscope with transport measurements.[26] A representative photocurrent map measured from a p-i-n SiNW (Figure 3a) shows a large photocurrent in the middle region of the device, where the position of the SiNW devices is highlighted by registered SEM image overlaid on the photocurrent data. Analysis of the photocurrent peaks yield a full-width-half-maximum (fwhm) of ca. 500 nm perpendicular to the nanowire axis, which corresponds to the upper bound on the spatial resolution of our measurements. The fwhm along the SiNW axis, ca. 1.5 μm, is consistent with the length of the i-region characterized independently by SGM and EFM.

The photocurrent in the middle region of our p-i-n SiNW devices has a peak value typically 10^2-10^3 times (500 in Figure 3a) larger than the photocurrents measured on the p- and n-regions. This observation is consistent with the large potential drop and corresponding strong electric field in the i-region, which can efficiently separate photogenerated electron−hole pairs to create a photocurrent. In addition, negligible photocurrent response is observed at the SiNW−metal contacts, which is distinct from previous studies where Schottky barriers dominate the response.[9,27] These results demonstrate clearly that the active detecting region is localized at the i-region of the p-i-n SiNWs.

To determine the avalanche multiplication in the i-region, we measured the dark current (I_{dark}) and the photocurrent (I_{ph}) from the center of the i-region of p-i-n SiNW devices as a function of reverse bias voltage as shown in Figure 3b. At the levels of illumination used in our experiments, the I_{ph} is up to 10^2 larger than the I_{dark} and increases with increasing reverse bias. Avalanche gain is quantified by calculating the avalanche multiplication factor, M, defined as $M = I_{ph}/I_{ph0}$, where I_{ph0} is the primary unmultiplied photocurrent at the bias voltage at which the I_{ph} is measured.[15,16] The value of I_{ph0} is obtained from a linear extrapolation of the I_{ph} in the bias region of from 20 to 25 V where the curve is nearly flat. The plot of M versus reverse bias voltage (red curve, Figure 3b) shows that this device exhibits a multiplication factor of ca. 30 for sub-breakdown biases. Similar values of M have been reproducibly observed in a number of p-i-n SiNW devices, and moreover, we note that these values are comparable to multiplication factors for planar Si APDs.[16]

In addition, the responsivity of the p-i-n SiNW photodectors was measured as a function of the incident laser power. I_{ph} vs laser power (Figure 3c) measured at 22, 20, and 18 V show linear dependences with slopes of 1.16, 0.94, and 0.72 nA/μW, respectively. As expected, larger I_{ph} values are observed for larger reverse bias voltages at the same incident laser power. The responsivity of SiNW devices is limited by optical absorption and geometric effects; for example, only ca. 0.02% of the incident light is absorbed by a 20 nm SiNW photoexcited with a 500 nm fwhm beam with 0.9 μm absorption length. If we correct for these limitations on

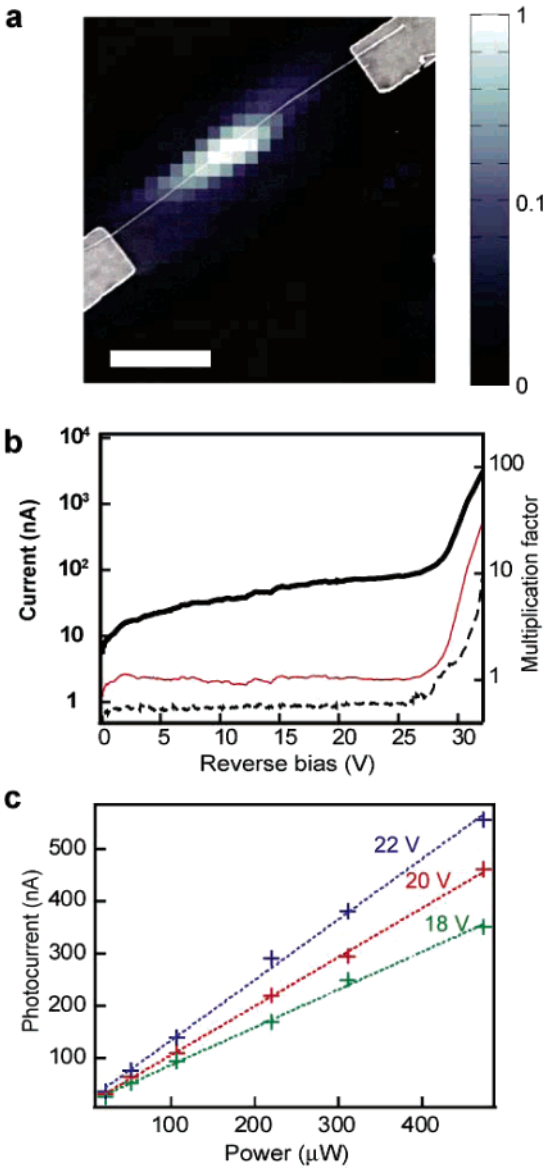

Figure 3. Photocurrents from p-i-n SiNW avalanche photodiodes. (a) Normalized photocurrent map with superimposed SEM image of a 20 nm p-i-n SiNW. The length of the intrinsic region determined by EFM, and SGM is 1.5 μm. The bias voltage and the scanning step size were −28 V and 250 nm (in x and y), respectively. Scale bar, 2 μm. (b) Photocurrent (black solid line), dark current (dashed line) $I-V$ data, and corresponding multiplication factor (red line). (c) Photocurrent vs optical power at 488 nm for reverse bias values of 22 V (blue line), 20 V (red line), and 18 V (green line). (b) and (c) were measured with the laser focused onto the center of the intrinsic region.

absorption in p-i-n SiNW photodectors, the responsivity is comparable to values for planar Si APD devices.[16] By operation of the device in the Geiger mode,[28] the sensitivity could be substantially increased to overcome intrinsic geometric and absorption limitations.

We have also investigated the multiplication factors for holes and electrons by local photoexcitation[21] of the p-type or n-type regions of p-i-n SiNW devices as shown in panels a and b of Figure 4.[29] The I_{ph} versus reverse bias voltage results shown in Figure 4c demonstrate that the photocurrents are larger than the dark current (black curve) and increase

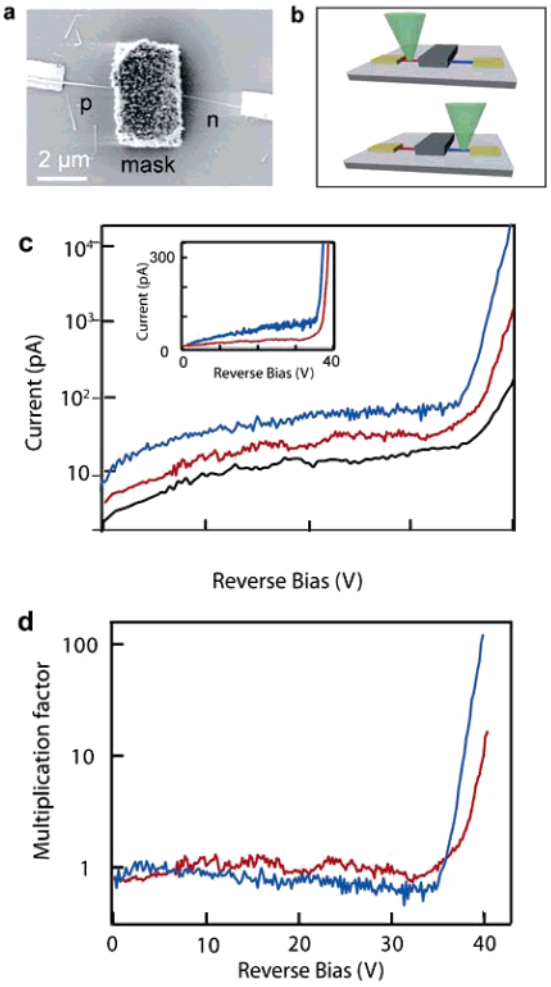

Figure 4. Measurement of the multiplication factors for electrons and holes in p-i-n SiNW devices. (a) SEM image of a p-i-n SiNW device with the i-region masked by a thick high optical density polymer.[29] Scale bar, 2 μm. (b) Schematics of localized laser excitation of the p- and n-type regions. (c) I_{ph} (red, blue curves) and I_{dark} (black curve) vs reverse bias voltage. The blue and red curves correspond to I_{ph} recorded with local photoexcitation of the p- and the n-regions, respectively; dark current was subtracted from I_{ph}'s. (d) Multiplication factors calculated as functions of reverse bias for electrons (blue) and holes (red), respectively.

with increasing of voltage, when laser excitation is on either p-region (blue curves) or n-region (red curves). In addition, the photocurrent measured with local excitation of the p-region is larger than that observed from local excitation of the n-region over the whole range of reverse bias voltages studied (Figure 4c).[30] These results indicate that the multiplication factor for electrons, the minority carriers injected into the high-field i-region upon photoexcitation of the p-region, is larger than that for holes.

These data have been used to determine the multiplication factors for electron and hole injections, M_n and M_p, respectively. The multiplication factors are defined as $M_n = I_{ph}/I_{n0}$ and $M_p = I_{ph}/I_{p0}$, where I_{n0} (I_{p0}) is the primary photocurrent (i.e., with unity gain) under the condition of pure electron (hole) injection.[21] I_{n0} and I_{p0} are obtained from a linear extrapolation of the photocurrent data at biases below the onset of avalanche breakdown (inset, Figure 4b). This linear extrapolation somewhat underestimates M_n; an accurate

evaluation of the latter would require a detailed physical model for the voltage dependence of I_{n0}. As shown in Figure 4d, M_n reaches a value of ca. 100 while M_p is ca. 20 when the applied bias is approaching the breakdown voltage. This implies that the ionization rate for electrons is significantly higher than that for holes in agreement with a large body of work in silicon avalanche devices.[15,21,31,32] It has been a well-known fact that, in p-i-n junctions with constant electric field, simple analytical expression can be established to relate the ionization rate of electrons (α) and holes (β) and M_n and M_p, which allows one to determine α and β as a function of electric fields.[21] We have not followed this procedure here since accurate knowledge of the field distribution along the SiNW, which may cause a large error in the determination the ionization rates due to their exponential dependence on the electric field, is not known. Accurate measurements of α and β could provide crucial information for understanding carrier−phonon interactions at high electric fields[33] and, in sufficiently small diameter SiNWs, the dependence of impact ionization on crystal orientation.[21] Such experiments might also shed light on the effect of optical phonon confinement on ionization coefficients in SiNWs.[34]

In summary, we have described a general and controlled approach for synthesizing single-crystal p-i-n SiNW structures. High-resolution TEM, EFM, and SGM were used to spatially define the structure and electrical properties of the three regions along the SiNW p-i-n structures. Temperature-dependent transport measurements were used to characterize the diode behavior and demonstrated an avalanche breakdown mechanism at large reverse bias. In addition, photocurrent measurements show that p-i-n SiNW devices act as nanoscale APDs with a spatial resolution defined by the physical dimension of the i-region encoded during growth. Photomultiplication as well as pure multiplication factors for electrons and holes were determined and found to be comparable to published results for planar Si APDs. These p-i-n SiNW APDs should make possible integrated nanophotonic systems, by providing direct polarization sensitivity, high spatial resolution, and high sensitivity not achievable with conventional planar photodetectors, and, moreover, the capability of being readily assembled with other distinct photonic elements in a bottom-up approach.[1a,7a] In addition, the nanowire APDs will enable access to new and interesting physics associated with confined one-dimensional or quasi-one-dimensional semiconducting systems, such as investigations of impact ionization rates, as carrier−phonon interactions change due to confinement. Last, while our studies have focused on characterizing the fundamental properties of individual p-i-n SiNW devices, emerging assembly techniques[35] could be used to fabricate large arrays of addressable p-i-n SiNW APDs over flexible or rigid substrates thus enabling a variety of additional applications.

Acknowledgment. We thank Professor X. Zhuang for the use of the scanning optical microscope system. F.C. acknowledges support from the NSF Nanoscale Science and Engineering Center and the Harvard Center for Nanoscale Systems (CNS). C.M.L. acknowledges support of the Air Force Office of Scientific Research.

References

(1) (a) Lieber, C. M. *MRS Bull.* **2003**, *28*, 486. (b) Yang, P. *MRS Bull.* **2005**, *30*, 85.
(2) (a) Duan, X.; Huang, Y.; Cui, Y.; Wang, J.; Lieber, C. M. *Nature* **2001**, *409*, 66. (b) Zhong, Z.; Qian, F.; Wang, D.; Lieber, C. M. *Nano Lett.* **2003**, *3*, 343. (c) Huang, Y.; Duan, X.; Lieber, C. M. *Small* **2005**, *1*, 142.
(3) (a) Qian, F.; Li, Y.; Gradeak, S.; Barrelet, C. J.; Wang, D.; Lieber, C. M. *Nano Lett.* **2004**, *4*, 1975. (b) Kim, H.; Cho, Y.; Lee, H.; Kim, S.; Ryu, S. R.; Kim, D. Y.; Kang, T. W.; Chung, K. S. *Nano Lett.* **2004**, *4*, 1059. (c) Qian, F.; Gradecak, S.; Li, Y.; Wen, C.-Y.; Lieber, C. M. *Nano Lett.* **2005**, *5*, 2287.
(4) (a) Huang, M. H.; Mao, S.; Feick, H.; Yan, H.; Wu, Y.; Kind, H.; Weber, E.; Russo, R.; Yang, P. *Science* **2001**, *292*, 1897. (b) Johnson, J. C.; Choi, H. J.; Knutsen, K. P.; Schaller, R. D.; Yang, P.; Saykally, R. J. *Nat. Mater.* **2002**, *1*, 106.
(5) Duan, X.; Huang, Y.; Agarwal, R.; Lieber, C. M. *Nature* **2003**, *421*, 241.
(6) (a) Agarwal, R.; Barrelet, C. J.; Lieber, C. M. *Nano Lett.* **2005**, *5*, 917. (b) Gradecak, S.; Qian, F.; Li, Y.; Park, H.-G.; Lieber, C. M. *Appl. Phys. Lett.* **2005**, *87*, 173111.
(7) (a) Barrelet, C. J.; Greytak, A. B.; Lieber, C. M. *Nano Lett.* **2004**, *4*, 1981. (b) Law, M.; Sirbuly, D. J.; Johnson, J. C.; Goldberger, J.; Saykally, R. J.; Yang, P. *Science* **2004**, *305*, 1269.
(8) Greytak, A. B.; Barrelet, C. J.; Li, Y.; Lieber, C. M. *Appl. Phys. Lett.* **2005**, *87*, 151103.
(9) (a) Wang, J.; Gudiksen, M. S.; Duan, X.; Cui, Y.; Lieber, C. M. *Science* **2001**, *293*, 1455. (b) Kind, H.; Yang, P.; Yan, H.; Messer, B.; Law, M. *Adv. Mater.* **2002**, *14*, 158. (c) Ahn, Y.; Dunning, J.; Park, J. *Nano Lett.* **2005**, *5*, 1367. (d) Gu, Y.; Kwak, E. S.; Lensch, J. L.; Allen, J. E.; Odom, T. W.; Lauhon, L. J. *Appl. Phys. Lett.* **2005**, *87*, 043111.
(10) Hayden, O.; Agarwal, R.; Lieber, C. M. *Nat. Mater.* **2006**, *5*, 352.
(11) Barrelet, C. J.; Bao, J.; Loncar, M.; Park, H.; Capassos, F.; Lieber, C. M. *Nano Lett.* **2006**, *6*, 11.
(12) Lukosz, W. *Sens. Actuators, B* **1995**, *29*, 37.
(13) Vilkner, T.; Janasek, D.; Manz, A. *Anal. Chem.* **2004**, *76*, 3373.
(14) Miller, D. A. B. *Proc. IEEE* **2000**, *88*, 728.
(15) Sze, S. M. *Physics of Semicoductor Devices*; Wiley: New York, 1981.
(16) Kasap, S. O. *Optoelectronics and Photonics: Principles and Practices*; Prentice Hall: Upper Saddle River, NJ, 2001.
(17) Samuelson, L.; Thelander, C.; Bjork, M. T.; Borgstrom, M.; Deppert, K.; Dick, K. A.; Hansen, A. E.; Martensson, T.; Panev, N.; Persson, A. I.; Seifert, W.; Skold, N.; Larsson, M. W.; Wallenberg, L. R. *Physica E* **2004**, *25*, 313.
(18) Yang, C.; Zhong, Z.; Lieber, C. M. *Science* **2005**, *310*, 1304.
(19) (a) The p-type and n-type regions were synthesized with B_2H_6:SiH_4 = 1:100 and PH_3:SiH_4 = 1:100. Effective carrier concentrations were estimated based on four probe transport measurements at room temperature. (b) Wu, Y.; Xiang, J.; Lu, W.; Lieber, C. M. *Nature* **2004**, *430*, 61.
(20) Wu, Y.; Cui, Y.; Huynh, L.; Barrelet, C. J.; Bell, D. C.; Lieber, C. M. *Nano Lett.* **2004**, *4*, 433.
(21) Capasso, F. The Physics of Avalanche Photodiodes. In Tsang, W. T. *Semiconductors and Semimetals*, Vol. 22., Part D.; Willardson, R. K., Beers, A. C., Eds.; Academic Press: Orlando, FL, 1985.
(22) Kaneda, T.; Mikawa, T.; Toyama, Y.; Ando, H. *Appl. Phys. Lett.* **1979**, *34*, 692.
(23) Bonnell, D. A., *Scanning Probe Microscopy: Theory and Applications*; John Wiley & Sons: New York, 2000.
(24) Bachtold, A.; Fuhrer, M. S.; Plyasunov, S.; Forero, M.; Anderson, E. H.; Zettl, A.; McEuen, P. L. *Phys. Rev. Lett.* **2000**, *84*, 6082.
(25) All p-i-n devices were fabricated on heavily doped Si substrates with 50-nm thermal oxide (n-type, resistivity <0.005 Ω•cm, Nova Electronic Materials, Carrollton, TX). Nickel contacts (60 nm thick) at the p- and n-type ends of individual SiNWs were patterned by electron beam lithography and deposited by thermal evaporation. The contacts were annealed at 350 °C for 30 s. EFM and SGM measurements were carried out with a Nanoscope IIIa and metal-coated tips (Nanosensor) with radii of curvature of 10−30 nm. EFM and SGM data were acquired in lift mode (lift height = 150 and 15 nm for EFM and SGM, respectively) with V_{sd} = 1 V and V_{tip} = 9 V. In EFM measurements, the electrostatic force between the nanowire

and the AFM tip results in a phase shift, $\Delta\varphi \propto (d^2C/dz^2)(V_{tip} + \phi - V_{sd})^2$, where C is the tip−sample capacitance, z is the tip−sample separation, and ϕ is the work function difference between tip and sample.[24] A plot of $\Delta\varphi$ vs position thus provides a measure of the potential drop along the SiNW. In SGM measurements, the tip functions as a local gate ($V_{gate} = V_{tip}$) and the conductance vs position provides a measure of local accumulation or depletion of carriers.[18,24]

(26) The 488 nm excitation beam of an Ar-ion laser, focused to a diffraction-limited focal spot by a 0.9-NA objective microscope, is used to locally photoexcite the p-i-n SiNW. When the p-i-n SiNW is operated at reverse bias, a photocurrent is detected when the laser impinges on the p-i-n SiNW. The piezo-controlled sample stage (Digital PI PZT flexure stage) is then used to scan the sample from point to point to spatially map out the photocurrent. The current was measured in the dark and under dc illumination conditions using a parameter analyzer (Agilent 4156c). The incident optical power level was kept large enough to ensure that the dark current is negligible compared to the photocurrent in the bias range of the experiments.

(27) Ahn, Y.; Dunning, J.; Park, J. *Nano Lett.* **2005**, *5*, 1367.

(28) Brown, R. G. W.; Ridley, K. D.; Rarity, J. G. *Appl. Opt.* **1986**, *25*, 4122.

(29) Local photoexcitation of either the p- or n-regions, which enables minority carrier injection of electrons and holes, respectively, into the i-region, was carried out using a diffraction limited laser spot with a fwhm of ca. 500 nm. Furthermore, to prevent direct photoexcitation of the i-region, we lithographically masked this section of the sample with a high optical density polymer (PSK2000, Brewer Science, Inc.); the 1.5 μm thickness used has a 99.9% absorption at the excitation wavelength, 488 nm, used in our experiments.

(30) Careful comparison of the p-i-n SiNW devices shown in Figures 3b and 4c shows some difference in the reverse bias characteristics. In Figure 3b, we observe an essentially constant I_{dark} vs bias up to the onset of avalanche multiplication. This behavior is expected for an ideal p-i-n device. The device shown in Figure 4c shows, however, a small increase in I_{dark} vs revserse bias before the gain onset is reached. It is an interesting question to explore if this breakdown voltage might be limited by a microplasma mechanism, since in the SiNW devices the field is *by design* localized to a nanoscale size spot (20 nm diameter). Microplasma breakdown can occur in localized spots in avalanche devices, as opposed to bulk breakdown, which occurs at higher bias in silicon.[15] Overall these data are consistent with the expected behavior of bulk p-i-n Si devices, although future more detailed studies might reveal interesting differences.

(31) Agarwal, P.; Goossens, M. J.; Zieren, V.; Aksen, E.; Slotboom, J. W. *IEEE Electron Device Lett.* **2004**, *25*, 807.

(32) Massey, D. J.; David, J. P. R.; Tan, C. H.; Ng, B. K.; Rees, G. J.; Robbins, D. J.; Herbert, D. C. *J. Appl. Phys.* **2004**, *95*, 5931.

(33) Baraff, G. A. *Phys. Rev.* **1962**, *128*, 2507.

(34) (a) Piscanec, S.; Cantoro, M.; Ferrari, A. C.; Zapien, J. A.; Lifshitz, Y.; Lee, S. T.; Hofmann, S.; Robertson, J. *Phys. Rev. B* **2003**, *68*, 241312. (b) Fukata, N; Oshima, T.; Murakami, K. *Appl. Phys. Lett.* **2005**, *86*, 213112. (c) Adu, K. W.; Gutierrez, H. R.; Kim, U. J.; Sumanasekera, G. U.; Eklund, P. C. *Nano Lett.* **2005**, *5*, 409.

(35) Jin, S.; Whang, D.; McAlpine, M. C.; Friedman, R. S.; Wu, Y.; Lieber, C. M. *Nano Lett.* **2004**, *4*, 915.

NL062314B